ANNUAL REVIEWS

Annual Review of Environment and Resources

The Ocean Carbon Cycle

Tim DeVries

Department of Geography and Earth Research Institute, University of California, Santa Barbara, California, USA; email: tdevries@geog.ucsb.edu

Annu. Rev. Environ. Resour. 2022. 47:317–41

First published as a Review in Advance on July 25, 2022

The *Annual Review of Environment and Resources* is online at environ.annualreviews.org

https://doi.org/10.1146/annurev-environ-120920-111307

Keywords

carbon cycle, ocean carbon, CO_2 chemistry, carbon pumps, biological pump, anthropogenic CO_2

Abstract

The ocean holds vast quantities of carbon that it continually exchanges with the atmosphere through the air-sea interface. Because of its enormous size and relatively rapid exchange of carbon with the atmosphere, the ocean controls atmospheric CO_2 concentration and thereby Earth's climate on timescales of tens to thousands of years. This review examines the basic functions of the ocean's carbon cycle, demonstrating that the ocean carbon inventory is determined primarily by the mass of the ocean, by the chemical speciation of CO_2 in seawater, and by the action of the solubility and biological pumps that draw carbon into the ocean's deeper layers, where it can be sequestered for decades to millennia. The ocean also plays a critical role in moderating the impacts of climate change by absorbing an amount of carbon equivalent to about 25% of anthropogenic CO_2 emissions over the past several decades. However, this also leads to ocean acidification and reduces the chemical buffering capacity of the ocean and its future ability to take up CO_2. This review closes with a look at the uncertain future of the ocean carbon cycle and the scientific challenges that this uncertainty brings.

Contents

1. INTRODUCTION

Carbon plays a central role in Earth's life and climate systems. It is the basic currency of chemical energy in living organisms (1), and in the form of CO_2 is an important greenhouse gas in the atmosphere that helps to regulate Earth's climate (2, 3). The atmosphere and biosphere, however, are not the primary reservoirs of carbon in the Earth system (**Figure 1**). The largest reservoir of carbon is the solid Earth, which holds nearly 100,000 times as much carbon as the atmosphere, while the ocean is the second largest reservoir of carbon, with roughly 60 times as much carbon as the atmosphere. The exchange of carbon between these major reservoirs and the atmosphere and biosphere constitutes the global carbon cycle (**Figure 1**). Understanding and quantifying this cycle are among the primary aims of modern Earth system science.

The ocean plays a very important role in the global carbon cycle. It is the largest reservoir of carbon that readily exchanges with the atmosphere, and it hosts a diverse biosphere that cycles through nearly as much carbon as the entire terrestrial biosphere (**Figure 1**). Because of its vast size and relatively rapid exchange of CO_2 with the atmosphere, the ocean is the dominant natural control on atmospheric CO_2 concentrations on timescales of decades to millennia (16, 17). On very long timescales (>1 million years), the atmosphere, biosphere, and ocean can be considered one single carbon reservoir whose inventory is regulated by the immense reservoir of the solid Earth through weathering and volcanic activity (7). By contrast, rapid exchange with the terrestrial biosphere through photosynthesis and respiration controls the atmospheric CO_2 concentration on seasonal (18) to interannual timescales (19). This review therefore focuses on the intermediate timescales (decades to millennia), in which the ocean is the most important natural control on atmospheric CO_2.

Over the past 2,000 years, the atmospheric CO_2 concentration has exhibited two distinct modes (**Figure 2**). Prior to the start of the industrial revolution (~1780), the atmospheric CO_2 concentration was relatively steady at roughly 280 ppm. Over this multimillennial time span, the flows of carbon into and out of the atmosphere were closely balanced, and the atmospheric CO_2 concentration was regulated by exchange with a nearly unchanging ocean. Since then, the atmospheric CO_2 concentration has been steadily increasing due to the combustion of fossil fuels, which has powered economic development over the past 250 years (**Figure 2**). This industrial activity represents a massive acceleration in the natural release of carbon from geological reservoirs and has impacted all of the carbon reservoirs that exchange with the atmosphere, including the ocean.

The purpose of this review is to assess the state of the ocean carbon cycle and its role in regulating the atmospheric CO_2 concentration, both in the steady state of the preindustrial era and

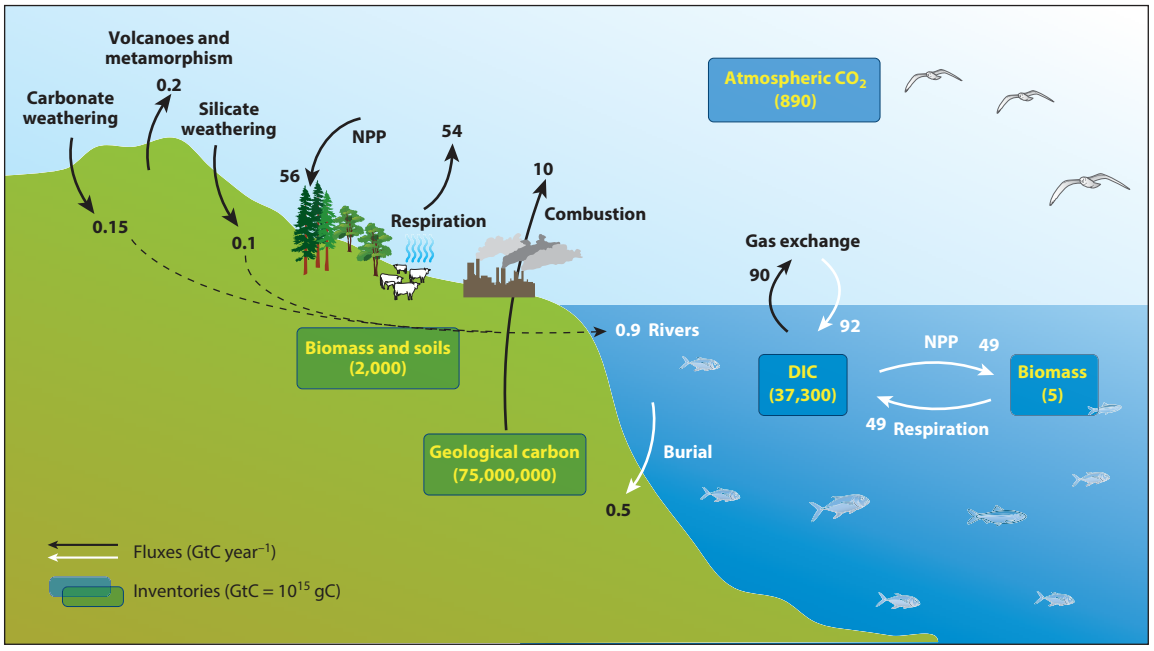

Figure 1

A schematic diagram illustrating Earth's contemporary carbon cycle (for the year 2020). Carbon inventories are based on estimates of geological carbon in limestone and shale rocks (including a comparatively small reservoir of fossil fuels) (4), carbon biomass in the ocean (5), the carbon inventory of terrestrial biomass and soils (5, 6), and atmospheric CO_2 and oceanic dissolved inorganic carbon (DIC) concentrations from contemporary observations (**Table 1**). Carbon fluxes between reservoirs are based on estimates of CO_2 emissions from volcanoes and metamorphism (7), CO_2 consumption by silicate weathering (8) and carbonate weathering (4), carbon burial in oceanic sediments (9), outflow of carbon from terrestrial environments to the ocean via rivers (10, 11), and release of CO_2 from fossil fuel combustion (12). Terrestrial net primary production (NPP) estimates are based on a meta-analysis (13), and terrestrial respiration is inferred as the residual between the contemporary net flux of CO_2 between the atmosphere and terrestrial biosphere from Reference 12 and the terrestrial NPP. Marine NPP estimates are based on a model from Reference 14, and marine respiration is assumed to be in balance with NPP due to a lack of direct estimates. Air-sea gas exchange fluxes are from the Global Carbon Budget 2020 (15). All of the numbers in this diagram are uncertain, with uncertainties ranging from ~10% (combustion, ocean and atmosphere carbon inventories) to ~30% (NPP, respiration, and gas exchange) to nearly 100% (river fluxes, weathering, and burial).

in its contemporary anthropogenically perturbed state. Accordingly, this review examines CO_2 chemistry in seawater and the equilibrium partitioning of CO_2 between the ocean and atmosphere (Section 2); the ocean carbon pumps and the mechanisms maintaining them (Section 3); and the response of the ocean to anthropogenic change, including through the oceanic uptake of anthropogenic CO_2 (Section 4). This review concludes with a look at the future of the ocean carbon sink and highlights some of the major gaps in our understanding of the ocean carbon cycle (Section 5).

There are aspects of the ocean carbon cycle that by necessity fall outside the scope of this review. These include interactions of the ocean dissolved inorganic carbon (DIC) reservoir with other carbon reservoirs that could regulate the ocean carbon inventory and ocean chemistry on multimillennial (>10,000 year) timescales, including the formation and dissolution of carbonate sediments (22), the cycling of carbon through methane hydrates in marine sediments (23), and carbon that is trapped in recalcitrant dissolved organic molecules in the ocean (24).

Dissolved inorganic carbon (DIC): the sum of dissolved CO_2, bicarbonate ion (HCO_3^-), and carbonate ion (CO_3^{2-}) in seawater

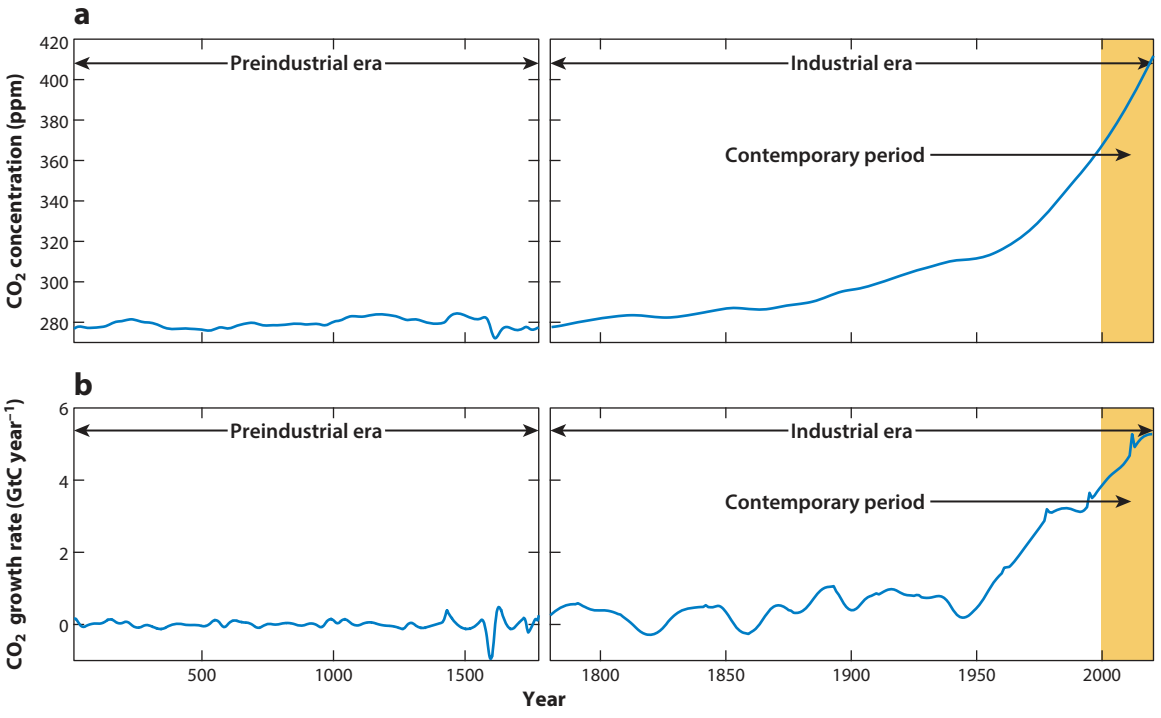

Figure 2

(*a*, *left*) Atmospheric CO_2 concentrations during the preindustrial era (0 AD to 1780) and (*right*) during the industrial era (1780 to present). Atmospheric CO_2 is based on ice core records from 0 AD to 1958 (20) and from direct measurements at the South Pole and Mauna Loa, Hawai'i, United States, from 1958 to 2020 (21). (*b*) The time rate of change of atmospheric CO_2, highlighting (*left*) a preindustrial steady state prior to 1780 AD (mean atmospheric CO_2 growth rate of 0 GtC year^{-1}) and (*right*) the positive growth rate of atmospheric CO_2 over the industrial era, reaching a value of 4.76 GtC year^{-1} in the contemporary period (2001–2020, *yellow*).

2. CO_2 SYSTEM CHEMISTRY AND THE EQUILIBRIUM PARTITIONING OF CARBON BETWEEN THE OCEAN AND ATMOSPHERE

The chemistry of CO_2 in seawater has been understood since the work of Buch in the 1930s (25, 26), with increasing analytical precision providing continued refinements to the understanding of the chemical equilibria of the CO_2 system in seawater (27, 28). This review does not examine these developments in detail but uses this well-established chemistry, along with some simplifications, to present a conceptual model for how seawater CO_2 chemistry influences the equilibrium partitioning of carbon between the ocean and atmosphere. This conceptual model demonstrates why the ocean has a far greater carbon inventory than does the atmosphere (**Figure 1**) and thus plays a major role in determining the atmospheric CO_2 concentration.

The air-sea exchange of CO_2 regulates the connection between the ocean and atmospheric carbon reservoirs. This exchange is driven by the diffusion of gaseous CO_2 across the air-sea interface (29), with the net exchange being proportional to the difference in the CO_2 gas pressure in air and seawater (30). Thus, it is closely tied to the solubility of CO_2 in seawater (K_0), which determines the ratio of CO_2 in aqueous solution in seawater to the partial pressure of CO_2 in the gas phase at chemical equilibrium:

$$K_0 = [CO_2]_{sw}/pCO_{2,sw}. \quad 1.$$

Equation 1 uses the partial pressure of CO_2 ($pCO_{2,sw}$, measured in microatmospheres) rather than the more accurate fugacity of CO_2, which takes into account the nonideal gas behavior of CO_2. The difference between partial pressure and fugacity is less than 1% (31) and is not important for the simple conceptual models proposed here. Likewise, the partial pressure of CO_2 is directly related to its atmospheric concentration (mole fraction, or xCO_2, measured in parts per million), and for dry air with a pressure of 1 atm the two are equivalent. For air with 100% humidity, the difference between pCO_2 and xCO_2 can be several percent (32). This review makes the simplifying approximation that the fugacity, partial pressure, and mole fraction are all equivalent and can be used interchangeably. While this is acceptable for developing an intuitive understanding, for more precise applications this may not be the case.

As CO_2 solubility increases, the concentration of CO_2 in aqueous solution increases for a given partial pressure of CO_2; conversely, the partial pressure of CO_2 in seawater decreases as the solubility increases for a given concentration of CO_2 in aqueous solution. Like most gases, the solubility of CO_2 increases as the seawater temperature decreases, such that polar waters with a temperature of 0°C have a solubility more than twice as large as that of equatorial waters with a temperature of 25°C (31). The solubility of CO_2 in seawater also depends on salinity, with higher-salinity waters having lower solubility, but the limited range of salinity in the ocean compared to temperature renders this effect small for most applications.

CO_2 also reacts with seawater to form carbonic acid, H_2CO_3, which then dissociates in two steps to bicarbonate, HCO_3^-, and carbonate, CO_3^{2-}, ions (28). The sum total of these is the DIC. The distribution of dissolved carbon across the three DIC species is closely related to the seawater pH (32). As pH decreases, the buffering capacity of seawater weakens (33) and the proportion of CO_2 relative to bicarbonate and carbonate ions increases, while increasing pH has the opposite effect. In the contemporary surface ocean, the pH is 8.11 ± 0.08 and the DIC/CO_2 ratio is 160 ± 50. This chemical speciation of CO_2 therefore effectively enhances the solubility of CO_2 by a factor of ~150, depending on the seawater pH. The resulting chemical equilibrium between DIC and seawater pCO_2 can be written as

$$\mathcal{F} = [\mathrm{DIC}]/pCO_{2,sw}. \quad 2.$$

This review refers to $\mathcal{F}$ as the seawater equilibrium carbon capacity. It is related to but distinct from the buffer or Revelle factor, R, in that $\mathcal{F}$ measures the equilibrium ratio of DIC to pCO_2, while R measures the ratio of the relative change in pCO_2 to the relative change in DIC (16, 34). It is therefore a measure of the equilibrium carbon balance rather than the response of the system to changes in that equilibrium. For conceptual convenience, when discussing the air-sea carbon balance, the units of $\mathcal{F}$ are mol air (kg seawater)$^{-1}$, which uses the approximation that $pCO_2 = xCO_2$.

Because seawater pH is tightly anticorrelated with pCO_2 for typical seawater pH ranges (35), $\mathcal{F}$ can be closely approximated as a function of $pCO_{2,sw}$. To examine the relationship between $\mathcal{F}$ and $pCO_{2,sw}$, seawater pCO_2 was calculated from measurements of seawater DIC and alkalinity from the Global Ocean Carbon Data Analysis Project version 2 (GLODAPv2.2021) (36) using the CO_2 chemistry calculator CO2SYS (37). The results show that $\mathcal{F}$ is a hyperbolic function of pCO_2 over the range commonly found in seawater (100–1,000 μatm) (**Figure 3**). A least squares fit shows that a hyperbola of the form

$$\mathcal{F} = 0.23 + 2{,}233/(pCO_2 + 34) \quad 3.$$

fits the observations with an R^2 of 0.98 and an RMS error of 0.18 mol air (kg seawater)$^{-1}$ (**Figure 3**). For a preindustrial CO_2 concentration of 280 ppm, the value of $\mathcal{F}$ is roughly 7.3 mol air (kg seawater)$^{-1}$. However, as pCO_2 increases, the value of $\mathcal{F}$ decreases (**Figure 3**). This coincides with a reduction of the carbon-buffering capacity of seawater at higher CO_2 concentrations

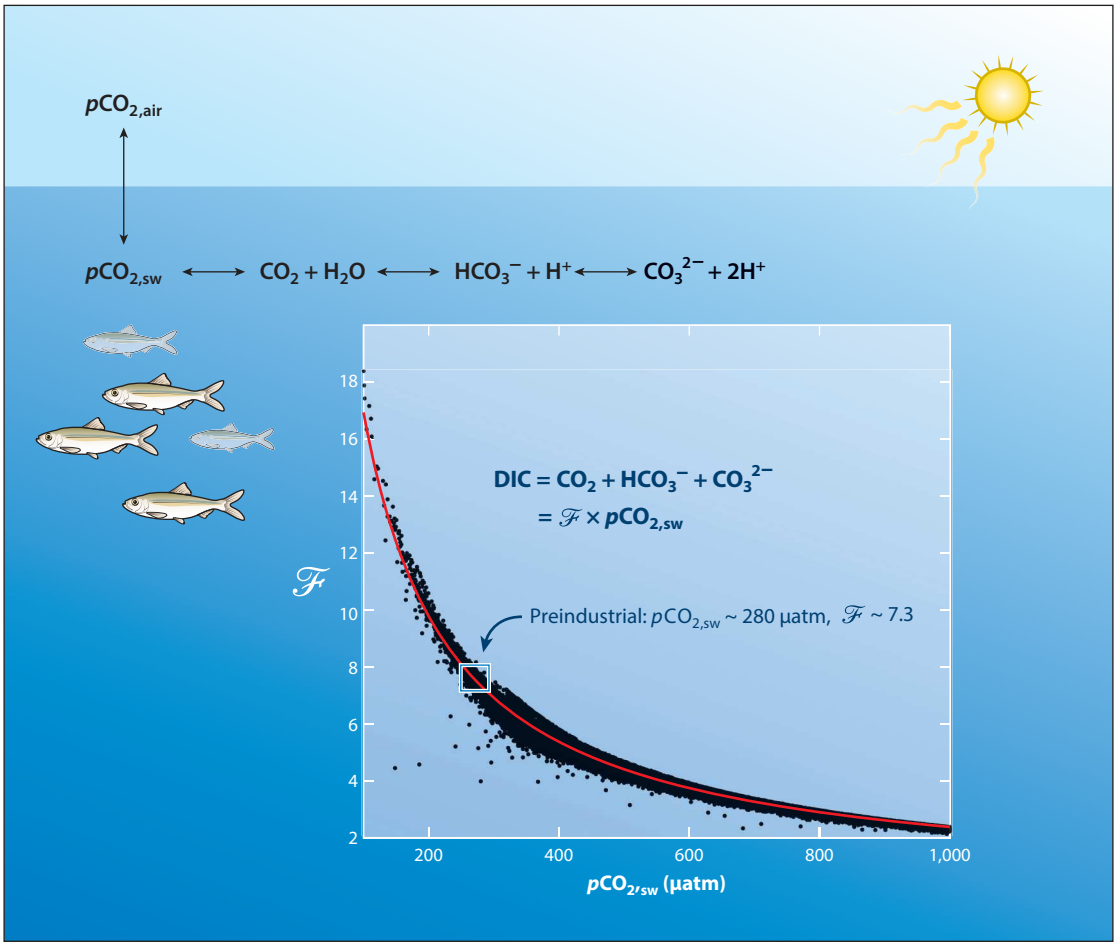

Figure 3

A schematic diagram illustrating a simple conceptual model of the ocean and atmosphere CO_2 exchange, in which the ocean is treated as a homogeneous carbon reservoir. The air-sea exchange of CO_2 is proportional to the difference in the partial pressure of CO_2 in the atmosphere ($pCO_{2,air}$) and seawater ($pCO_{2,sw}$). CO_2 in the ocean combines with water to form carbonic acid, which dissociates in two steps to form bicarbonate (HCO_3^-) and carbonate (CO_3^{2-}) ions. (*Inset*) Plot showing the relationship between the seawater equilibrium carbon capacity $\mathcal{F}$ (Equation 2) and seawater pCO_2 from contemporary observations. Abbreviation: DIC, dissolved inorganic carbon.

and lower pH (33). At a pCO_2 of ~600 µatm, the value of $\mathcal{F}$ is ~3.5, representing roughly a halving of the equilibrium carbon capacity of seawater for a doubling of the pCO_2.

The impact of this chemistry on the partitioning of carbon between the ocean and atmosphere can be illustrated using a simple two-box model of the ocean-atmosphere system. In this simple system, the ocean is approximated as a single well-mixed reservoir of DIC, with a concentration of $\overline{\mathrm{DIC}}$. In this system, the total carbon inventory of the ocean is

$$C_{oce} = M_{oce}\overline{\mathrm{DIC}}, \quad 4.$$

while the total carbon inventory of the atmosphere is

$$C_{atm} = M_{atm} pCO_{2,air}, \quad 5.$$

Table 1 Metrics of the ocean and atmosphere carbon cycle

Quantity (units)	Value		Meaning
	Preindustrial	Contemporary	
M_{oce} (kg)	1.38×10^{21}	1.38×10^{21}	Mass of the ocean[a]
M_{atm} (mol)	1.77×10^{20}	1.77×10^{20}	Molar mass of the atmosphere[b]
$xCO_{2,air}$ (ppm)	280	410	Atmospheric CO_2 concentration
DIC_s (μmol kg^{-1})	2,040	2,090	Average surface[c] seawater DIC
DIC_d (μmol kg^{-1})	2,250	2,260	Average deep ocean[d] DIC
$\mathcal{F}$ [mol air (kg seawater)$^{-1}$]	7.2	–[e]	Ratio of DIC/xCO_2 at chemical equilibrium
C_{oce} (GtC)	37,100[f]	37,300[g]	Total mass of inorganic carbon in the ocean
C_{atm} (GtC)	595	890	Total mass of carbon as CO_2 in the atmosphere

Abbreviations: DIC, dissolved inorganic carbon; GLODAPv2.2021, Global Ocean Carbon Data Analysis Project version 2.
[a]Assuming a global ocean volume of 1.34×10^{18} m^3 from Reference 39 and a mean density of 1,036 kg m^{-3}.
[b]Using the mass of the dry atmosphere is 5.135×10^{18} kg (40) and molar mass of dry air is 2.896 g mol^{-1}.
[c]0–200 m.
[d]200 m to seafloor.
[e]Value is not given because the ocean-atmosphere system is not presently at chemical equilibrium.
[f]Based on a mean ocean DIC value of 2,248 μmol kg^{-1} from GLODAPv2.2021 (36) corrected for anthropogenic DIC from Reference 41.
[g]Based on a mean ocean DIC value of 2,248 μmol kg^{-1} from GLODAPv2.2021 (36).

with M_{oce} the mass of the ocean and M_{atm} the molar mass of the dry atmosphere (**Table 1**). The timescale for this system to come to equilibrium through air-sea gas exchange is roughly 40 years (scaling the estimate of Reference 38 of ~1 year for a 100-m mixed layer to the full ocean depth), and thus such a system could easily be in equilibrium at a preindustrial steady state (**Figure 2**); in this equilibrium state, the seawater pCO_2 and atmospheric pCO_2 would be identical. Assuming equilibrium, combining Equations 2, 4, and 5 yields the following expression for the ratio of the size of the oceanic and atmospheric carbon reservoirs:

$$\frac{C_{oce}}{C_{atm}} = \mathcal{F}\frac{M_{oce}}{M_{atm}}. \quad 6.$$

The ratio of the mass of the ocean to the molar mass of the atmosphere is 7.8 kg seawater (mol air)$^{-1}$ (**Table 1**).

The simple expression in Equation 6 implies that, to first order, the partitioning of carbon between the ocean and atmosphere depends on the relative masses of the ocean and the atmosphere and on the equilibrium carbon capacity of seawater, i.e., $\mathcal{F}$. Equation 6, along with the simplified expression for the carbon capacity of seawater in Equation 3, implies that at an atmospheric pCO_2 of 280 μatm, the ratio of DIC to pCO_2 would be 7.3 and the ratio of C_{oce} to C_{atm} would be roughly 56. This can be checked against the preindustrial oceanic DIC inventory, which is ~37,100 GtC (**Table 1**), and the preindustrial atmospheric carbon inventory of ~595 GtC, for a ratio of ~62. The theoretical ratio derived from the two-box model is slightly less than the observed ratio but within the same ballpark, illustrating the utility of this simple conceptual approach for understanding the partitioning of carbon between the ocean and atmosphere. However, if one specifies the total carbon inventory of the ocean/atmosphere system at a preindustrial value of 3.2×10^{18} mol C, Equations 3 and 6 imply an atmospheric pCO_2 of 583 ppm, roughly twice the preindustrial value of 280 μatm. Clearly, the two-box model is not entirely sufficient for understanding

the equilibrium partitioning of carbon between the ocean and atmosphere, and even greater errors are introduced when using this simple conceptual model to deduce the atmospheric CO_2 concentration at equilibrium.

Last glacial maximum: the period from roughly 18,000 to 25,000 years before present, when the atmospheric CO_2 concentration was about 80–100 ppm lower than during the preindustrial period and the average Earth surface temperature was roughly 5°C colder

3. THE OCEAN CARBON PUMPS

In the simple system considered in **Figure 3**, the ocean is a well-mixed reservoir of inorganic carbon exchanging with the atmosphere. In this simple system, the partitioning of carbon between the ocean and atmosphere is determined by the equilibrium carbon capacity of the CO_2 system and the relative masses of the ocean and atmosphere. However, the real ocean is more complex. The most important point neglected in that simple conceptual framework is that there are substantial gradients in DIC in the ocean, in particular a strong vertical gradient with relatively low DIC concentrations near the surface and higher concentrations at depth (**Figure 4**). These gradients are maintained by the ocean carbon pumps, primarily the solubility and biological carbon pumps (42), which are reviewed in Sections 3.1 and 3.2. The ocean carbon pumps play an important role in regulating the partitioning of carbon between the ocean and atmosphere, and variations in their strengths are expected to be the main driver of variations in atmospheric CO_2 on the timescales of millennia. For example, a stronger carbon pump is thought to be responsible in some capacity for the much lower atmospheric CO_2 concentration during the last glacial maximum (43–45).

The influence of the carbon pumps on the partitioning of carbon between the atmosphere and ocean can be illustrated by revisiting the simple two-box ocean-atmosphere model of Section 2 but dividing the ocean into surface and deep layers. The difference between the surface and deep ocean DIC concentration in the contemporary ocean is about 170 μmol kg^{-1}, and in the preindustrial ocean the gradient is over 200 μmol kg^{-1} (**Table 1**; **Figure 4**). In this system, the total ocean carbon inventory is the sum of the surface ocean and deep ocean inventories,

$$C_{oce} = M_{oce,s}\mathrm{DIC}_s + M_{oce,d}\mathrm{DIC}_d, \quad 7.$$

where the s and d subscripts refer to the surface and deep ocean, respectively. In this three-box model, the equilibrium partitioning of carbon between the ocean and atmosphere is

$$\frac{C_{oce}}{C_{atm}} = \mathcal{F}\left(\frac{M_s}{M_{atm}} + \frac{\mathrm{DIC}_d}{\mathrm{DIC}_s}\frac{M_d}{M_{atm}}\right). \quad 8.$$

Because the deep ocean volume is so much larger than the surface ocean volume that is equilibrated with the atmosphere, the simplifying assumption can be made that $M_s \to 0$ and $M_d \to M_{oce}$. Then the relationship simplifies to

$$\frac{C_{oce}}{C_{atm}} = \mathcal{F}\left(\frac{\mathrm{DIC}_d}{\mathrm{DIC}_s}\frac{M_{oce}}{M_{atm}}\right), \quad 9.$$

which is similar to the formula for the case in which the ocean is a homogeneous reservoir (Equation 6) but multiplied by the factor of the ratio of DIC in the deep ocean to that in the surface ocean. This ratio is about 1.1 in the preindustrial ocean (**Table 1**).

Using the parameters listed in **Table 1**, this simple three-box model (**Figure 4**) predicts a ratio of C_{oce} to C_{atm} of 62 for the preindustrial equilibrium state, which is very close to the ratio of 62.5 estimated from observations. Furthermore, if the total carbon content of the ocean and atmosphere is specified to be 3.2×10^{18} mol C, Equations 3 and 9 imply an atmospheric pCO_2 of 296 ppm, close to the preindustrial value of 280 μatm and roughly half the value predicted for the case of a homogeneous ocean. These considerations show that the existence of the ocean carbon pumps enhances the ocean carbon inventory by roughly 10% relative to a homogeneous ocean and reduces the atmospheric carbon inventory by a factor of 2. The approximately 10 times

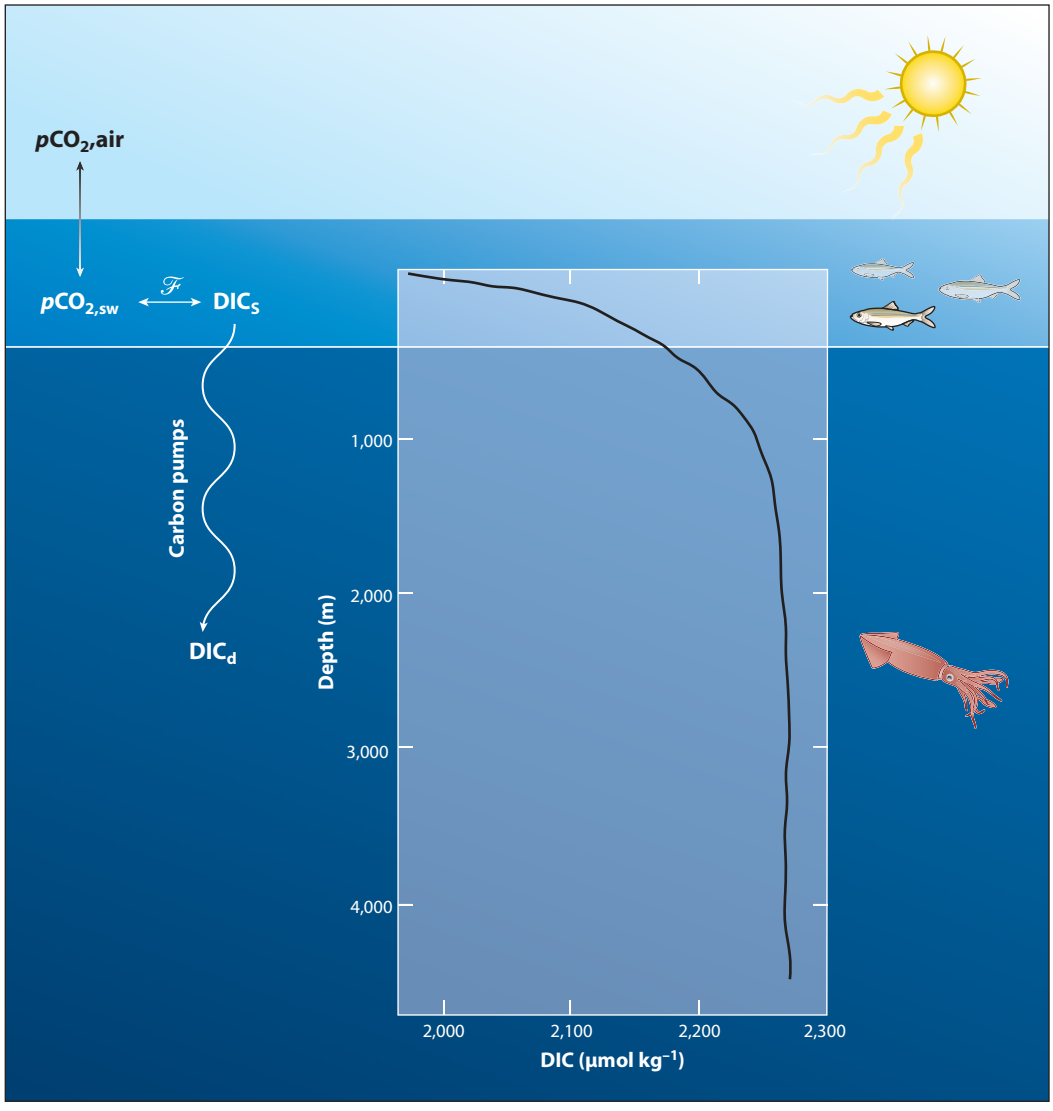

Figure 4

Schematic diagram of a simple conceptual model of the ocean and atmosphere CO_2 exchange, updated from **Figure 3** to separate the surface ocean that exchanges CO_2 with the atmosphere and the deep ocean that does not. Also shown is the increase in dissolved inorganic carbon (DIC) with depth in the contemporary ocean that is due to the ocean carbon pumps. $\mathcal{F}$ is the equilibrium carbon capacity of seawater (Equation 2).

greater leverage of the carbon pumps over atmospheric CO_2 than over the ocean carbon inventory is quantified by the Revelle (or buffer) factor of roughly 10 for the preindustrial ocean (16, 46).

The 1D conceptual model of **Figure 4** is sufficient to understand the effects of the carbon pumps on the equilibrium partitioning of carbon between the ocean and atmosphere but not how the pumps themselves operate. In the following section, I use oceanic DIC observations and an ocean carbon cycle model to illustrate how the solubility and biological pumps control the spatial distribution of DIC in the ocean and discuss the mechanisms by which they operate.

Thermocline: the region of the interior ocean underlying warm tropical and subtropical regions where the temperature rapidly decreases with depth

Net ecosystem productivity: the difference between autotrophic net primary productivity and heterotrophic respiration

3.1. Three-Dimensional Activities of the Solubility and Biological Carbon Pumps from Modern Observations

Deep and bottom waters of the ocean have an average temperature of roughly −2–4°C (47). These waters, which form in polar regions of the North Atlantic and in the Southern Ocean along the Antarctic shelf (48), have approximately twice the solubility of average surface waters, which have a temperature of roughly 20°C (31). The cold temperatures and enhanced solubility of the ocean's deep waters drive an increase in DIC with depth that is termed the solubility pump (42). The magnitude of the solubility pump depends on the volume of the deep ocean ventilated by cold, polar water masses compared to the (much smaller) volume of the oceanic thermocline that is ventilated by the wind-driven subtropical circulation (49) and on the degree of air-sea CO_2 disequilibrium in high-latitude regions (50, 51). Air-sea CO_2 disequilibrium typically reduces the magnitude of the solubility pump, because cold polar waters are often subducted into the deep ocean before reaching chemical equilibrium with the overlying atmosphere. When this happens, the deepwater masses have a deficit of DIC relative to what they would have at equilibrium, which reduces the effectiveness of the solubility pump (50, 52, 53).

The exact magnitude of the solubility pump in the ocean is impossible to observe directly, because the observed DIC distribution results from the convolved effects of solubility, air-sea CO_2 disequilibrium, the biological pump, and the invasion of anthropogenic CO_2 into the ocean. In this review, I separate these components using a global ocean carbon cycle model and modern observations of DIC in the ocean (41). The impact of the solubility pump can be diagnosed using a global ocean circulation model in which CO_2 exchanges with a well-mixed atmosphere with a fixed preindustrial atmospheric CO_2 concentration of 280 ppm, using a wind-speed-dependent model of CO_2 gas exchange rates (54). The resulting oceanic DIC distribution at steady state is called abiotic preindustrial DIC (**Figure 5*a–c***) and reflects the influence of the solubility pump in the preindustrial ocean under realistic gas exchange rates. The mean concentration of abiotic preindustrial DIC is roughly 2,065 μmol kg^{-1}, and the oceanic inventory of 34,230 GtC is approximately what would be expected from an ocean with a realistic thermal structure that is in equilibrium with the preindustrial atmospheric CO_2, with a slightly reduced DIC concentration due to CO_2 disequilibrium in cold deepwater formation regions (50). The thermal structure of the ocean determines the spatial gradients of DIC in this model, with the warm waters of the surface and thermocline having a DIC concentration of ∼2,030 μmol kg^{-1} and the coldest regions of the deep Southern Ocean having a DIC concentration close to 2,100 μmol kg^{-1} (**Figure 5*a*,*b***). The overall surface-to–deep ocean gradient of DIC with a realistic solubility pump is roughly 90 μmol kg^{-1} (**Figure 5*c***). If the ocean were in perfect equilibrium with atmospheric CO_2, the surface-to–deep ocean DIC gradient would be slightly larger at 150 μmol kg^{-1} and the oceanic DIC inventory would be about 2% greater, or approximately 34,960 GtC (**Figure 5*c***). Thus air-sea CO_2 disequilibrium reduces the carbon inventory of the preindustrial abiotic ocean by about 700 GtC.

The solubility pump accounts for roughly one-third of the vertical gradient of DIC in the ocean. The remainder is due to the so-called biological pump. The biological pump occurs due to the net ecosystem productivity of the surface ocean, which exports organic carbon into the deep ocean by a variety of mechanisms that are discussed in Section 3.2. The influence of the biological pump can be deduced by subtracting the abiotic preindustrial DIC from the observed DIC concentration, after correcting the observations for the invasion of anthropogenic CO_2 and the concentration and dilution of DIC resulting from evaporation and precipitation at the sea surface. The invasion of anthropogenic CO_2 can be quantified using model simulations (41) (see Section 4), while the concentration and dilution of DIC resulting from evaporation and precipitation can be accounted for by normalizing the DIC concentration to a common

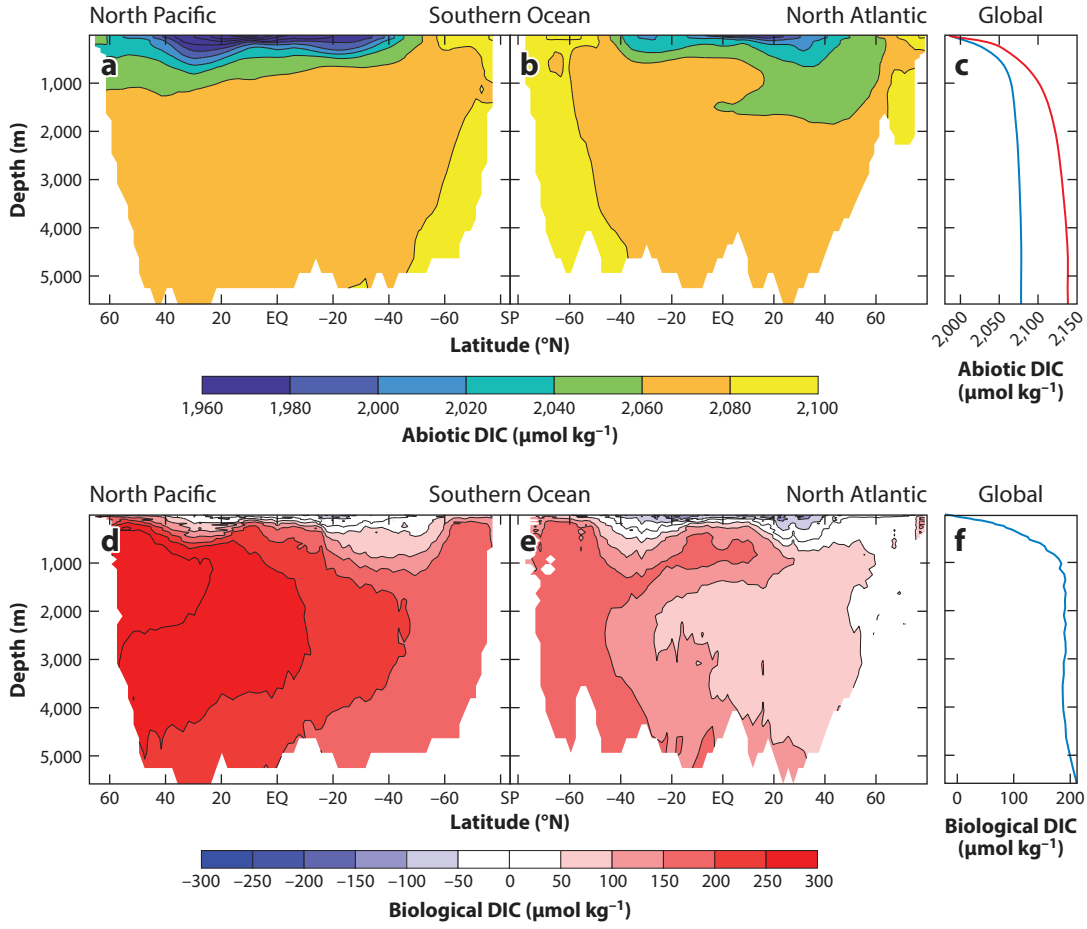

Figure 5

Preindustrial abiotic and biological DIC concentrations in the ocean. (*a–c*) Preindustrial abiotic DIC represents the distribution of DIC in a preindustrial ocean without biological processes, and the surface-to–deep ocean gradient in DIC (*c*) results solely from the solubility pump under realistic gas exchange. The red curve in panel *c* represents the vertical profile in DIC that would result if the ocean pCO_2 were fully equilibrated with the atmosphere. (*d–f*) Biological DIC is the difference between oceanic DIC in the preindustrial ocean and the preindustrial abiotic DIC (after correcting for the effects of precipitation and evaporation) and represents the influence of biological processes on the ocean DIC inventory. Abbreviations: DIC, dissolved inorganic carbon; EQ, equator; SP, South Pole.

reference salinity of 34.7 (55). After correcting for these factors, the resulting DIC concentration can be considered biological DIC (**Figure 5*d–f***), which traces out the integrated impacts of the biological pump on the ocean DIC concentration. Note that biological DIC is an excess or deficit of inorganic carbon due to biological processes in the ocean and is not similar to organic carbon, which is carbon fixed in organic molecules.

The presence of the biological pump leads to less DIC at the surface and more DIC in the deep ocean, adding an additional surface-to–deep ocean gradient of about 200 μmol kg^{-1} to the 90 μmol kg^{-1} present in the abiotic ocean (**Figure 5*d–f***). Biological DIC has a strong interbasin gradient, and it accumulates in the interior ocean as water masses age following the deep ocean conveyor circulation (56, 57). Deep waters in the North Atlantic are refreshed relatively rapidly, with ventilation ages on the order of a century or so (58), and these waters have the lowest biological DIC

Ventilation age: the time elapsed since water parcels in the interior ocean were last at the sea surface

Overturning circulation: the interconnected ocean currents that bring waters from the surface to the deep ocean and back again

concentrations of ~30–60 μmol kg^{-1}. The highest concentrations of biological carbon are found in the mid-depth North Pacific, coincident with the oldest ventilation ages in the ocean of around 1,400 years (59). Overall, the concentration of biological carbon in the ocean has a good correlation with ventilation age ($r = 0.87$). This general observation explains how changes in ocean ventilation can drive changes in the strength of the biological pump, with weaker overturning circulation leading to longer ventilation ages and a buildup of biological carbon in the interior ocean (60–62).

3.2. Mechanisms and Magnitude of the Biological Carbon Pump

Overall, the biological pump increases the inventory of DIC in the ocean relative to the case in which there is no biological pump. Based on the average biological DIC concentration of 170 μmol kg^{-1}, the global inventory of biological carbon in the ocean is roughly 2,800 GtC. This is roughly 8% of the ocean's total inorganic carbon inventory and is significantly larger than the total inventory of organic carbon in the ocean, which is ~600 GtC, most of which turns over relatively slowly, on the order of every 10,000 years (24).

The total amount of carbon stored in the ocean due to the biological pump is a combination of carbon both from respired organic matter, also known as the soft tissue pump (63), and from dissolved calcium carbonate ($CaCO_3$), also known as the carbonate pump (42). This separation is conceptually important, as different mechanisms govern the magnitudes of each of these pools of biological carbon. Also, while both pumps increase the accumulation of DIC in the interior ocean, they have opposing effects on seawater pCO_2. The formation of organic carbon by the soft tissue pump reduces seawater pCO_2 by removing DIC but leaving seawater pH relatively unchanged. In contrast, the formation of $CaCO_3$ reduces the seawater pH by effectively removing carbonate ions from solution, which has the effect of raising seawater pCO_2 (64).

The soft tissue biological pump results from the conversion of DIC to organic carbon by autotrophic net primary production (NPP) in the surface ocean, where sufficient light exists for photosynthesis. This euphotic zone extends to depths of roughly 30–150 m in the open ocean, depending on the water clarity (65). Global ocean NPP is approximately 50 GtC $year^{-1}$ (14, 66), but much of this NPP is metabolized by heterotrophic organisms in the euphotic zone and converted back to DIC. Roughly 20% of the NPP, or about 10 GtC $year^{-1}$ (67–70), escapes respiration in the euphotic zone and is transported into the deep ocean by a variety of mechanisms. Mechanisms of carbon export can be broadly classified as involving the gravitational settling of organic particles, the physical mixing of organic carbon into the ocean's deeper layers, or the vertical migrations of organisms between the euphotic zone and deeper layers (71). Organic particles that sink under the influence of gravity include the aggregates or flocculates of living or dead phytoplankton (72) and fecal pellets produced by zooplankton (73) and fish (74, 75). The physical mixing of organic carbon occurs due to the large-scale subduction (76) and the seasonal mixing (77) and eddy subduction (78) of water masses carrying particulate and dissolved organic carbon into the deeper ocean. Large populations of both zooplankton (79) and fish (80) reside at depths several hundred meters below the euphotic zone during the day and travel upward to the surface at night to feed. The downward migrations of these organisms transport organic carbon into the deeper ocean, where respiration and defecation release it back to the water column. The carbonate pump is carried out by organisms that synthesize carbonates, primarily $CaCO_3$, to form their hard exoskeletons. These include phytoplankton such as coccolithophores and foraminifera (81) and zooplankton such as pteropods (82). Calcifying benthic creatures such as crustaceans and mollusks do not contribute to the carbonate pump, because they live on the seafloor.

The summed effect of the soft tissue and carbonate biological pumps is to remove DIC from the surface and release it into the deeper water column, contributing to the buildup of biological

DIC in the deep ocean (**Figure 5**). The amount of carbon sequestered by the biological pump is determined by the sequestration time of remineralized DIC in the ocean (83). Each mechanism of the biological pump has a characteristic sequestration time that is determined by how deep the carbon is transported before being remineralized back to DIC (84) and on the regional ocean circulation patterns that return this carbon to the sea surface (83). The mean carbon sequestration time for the soft tissue pump is on the order of several hundred years (83), but it varies from a few years to several decades for dissolved carbon mixed into the thermocline to close to a millennium for carbon brought into the deep ocean well below the permanent thermocline (84).

Sequestration time: an analog of the ventilation age that measures the time elapsed during the transit of water parcels (and dissolved carbon in these parcels) from a location in the interior ocean to the sea surface

How much do the soft tissue and carbonate pumps contribute to the total ~2,800 GtC inventory of biological DIC? Carbon sequestration by the soft tissue pump can be estimated from nutrient and oxygen observations, taking advantage of the stoichiometric ratios of carbon, nutrients, and oxygen in marine organic matter (63, 85). Estimates based on oxygen and nutrient inventories suggest that the soft tissue pump sequesters around 1,300 GtC (86), a number that is supported by a data-constrained model of the biological pump (87). Analysis of the global alkalinity distribution suggests that the carbonate pump may sequester roughly 540 GtC (86). These estimates are based on the assumption that CO_2 instantaneously equilibrates with the atmosphere at the sea surface. However, this is not the case, because the chemical speciation of DIC in seawater leads to an air-sea equilibration time of roughly 1 year for a 100-m-deep surface mixed layer (38). The difference between the total biological carbon inventory and the estimated soft tissue and carbonate pumps is roughly 1,000 GtC of biological DIC, which can be attributed to air-sea CO_2 disequilibrium that enhances the effectiveness of the biological pump by preventing the immediate outgassing of biological DIC to the atmosphere in upwelling regions such as the Southern Ocean (88). This large role for air-sea disequilibrium in enhancing the effectiveness of the biological carbon pump is consistent with model simulations (88, 89). Note also that this increase in the biological carbon inventory of 1,000 GtC due to air-sea CO_2 disequilibrium more than counterbalances the −700 GtC weakening of the solubility pump due to air-sea disequilibrium, a conclusion that is in agreement with previous data-based calculations (90) and models (52).

4. THE OCEANIC SINK FOR ANTHROPOGENIC CARBON

About 90% of DIC in the ocean is due to the chemical equilibration of the ocean with the preindustrial atmosphere, which is only very slightly modified by air-sea disequilibrium (**Figure 5*a–c***). The second most important contributor to ocean DIC is the biological pump, which increases the ocean DIC inventory by roughly 10% (**Figure 5*d–f***). The third and smallest component of the contemporary ocean DIC reservoir is anthropogenic carbon, which is carbon that has been absorbed by the ocean in response to rising atmospheric CO_2 levels over the industrial era (91, 92) (**Figure 6*a***). Anthropogenic carbon cannot be observed directly due to its miniscule concentration in the ocean, but it can be estimated by various indirect methods that combine both observations and models (41, 93–95). One such estimate using an ocean circulation inverse model (41, 96) is shown in **Figure 6**. The model uses physical ocean circulation tracers to estimate the 3D global ocean circulation, and then uses this circulation model along with the atmospheric pCO_2 time history to calculate the invasion of anthropogenic CO_2 into the ocean. As of 2018, the ocean had accumulated ~185 Gt of DIC from the uptake of anthropogenic CO_2, representing an increase in the ocean DIC inventory of 0.5%.

Despite the small inventory of anthropogenic DIC in the ocean compared to that of the natural background, the oceanic uptake of anthropogenic CO_2 is extremely important because it helps to regulate Earth's climate response to CO_2 emissions (98). Humans have emitted 660 GtC (as of 2020) since the beginning of the industrial revolution through industrial activities

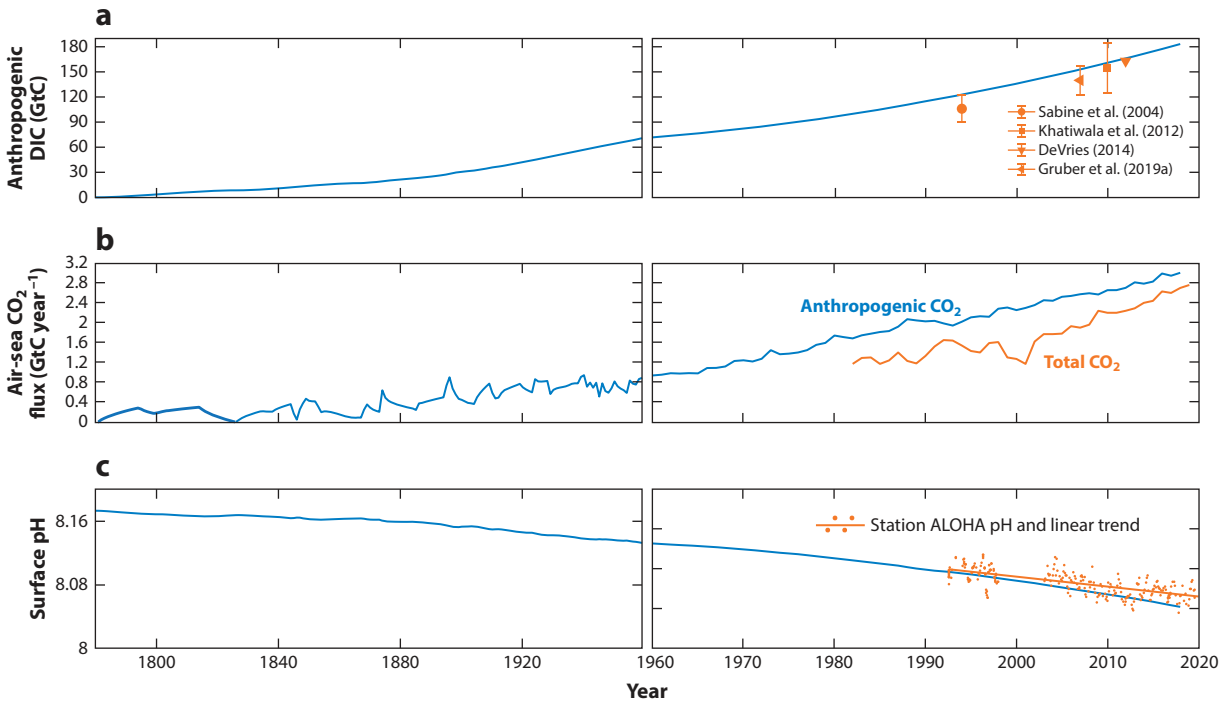

Figure 6

(*a*) Ocean anthropogenic dissolved inorganic carbon (DIC) accumulation over time from an ocean circulation inverse model (OCIM) (*blue trace*) compared with some prior estimates of the anthropogenic DIC inventory in the ocean. (*b*) Time evolution of air-sea anthropogenic CO_2 fluxes from OCIM (*blue trace*) and total CO_2 fluxes from the Global Carbon Budget 2020 (15) (*orange trace*). Positive values indicate net uptake of CO_2 by the ocean. (*c*) Average global surface ocean pH over time from OCIM, compared with pH measured near Hawai'i at Station ALOHA (97).

and deforestation (15), enough to raise the atmospheric CO_2 by over 300 ppm. But roughly 60% of these anthropogenic CO_2 emissions have been offset by increases in the carbon inventory of the ocean and the terrestrial biosphere (15), resulting in a more modest increase in atmospheric CO_2 of ∼130 ppm. The considerations addressed in Section 2 demonstrate that the ocean has a vast capacity to take up anthropogenic CO_2 once chemical equilibrium is reached, but its capacity is not unlimited. Due to a reduction of the equilibrium carbon capacity of the ocean at higher CO_2 levels (**Figure 3**), fossil carbon added to the atmosphere will not ultimately be divided among the ocean and atmosphere at the ∼62:1 ratio found in the preindustrial ocean. If the total anthropogenic CO_2 emissions were 100 Gmol C (roughly twice the amount that has so far been emitted), and the solubility and biological pumps remain unchanged, the simple three-box ocean-atmosphere model of Section 3 (Equations 3 and 9) predicts that this excess carbon will be distributed between the ocean and atmosphere at a ratio of only ∼7:1. Thus, much of the ocean's carbon-buffering capacity has already been exhausted, and the ocean can only be expected to take up ∼85% of anthropogenic CO_2 emissions at chemical equilibrium. This neglects any long-term dissolution of carbonate sediments, which could help to raise the buffering capacity of the ocean and thereby increase the uptake of anthropogenic CO_2 over tens of thousands of years (22).

In addition to its reduced equilibrium carbon capacity at higher CO_2 levels, the ocean takes up anthropogenic CO_2 much more slowly than would be assumed from its relatively rapid air-sea equilibration time. This is because the rate of anthropogenic CO_2 uptake is limited not by

gas exchange but by the rate of the ocean's overturning circulation, which determines the rate at which deep waters that are free of anthropogenic CO_2 are exposed at the sea surface (99). Because the ocean's overturning timescale is on the order of 1,000 years, it will take millennia before chemical equilibrium is reached between the atmosphere and the ocean. The contemporary uptake of anthropogenic CO_2 by the ocean is roughly 2.5 GtC year^{-1} (**Figure 6*b***), equivalent to about 25% of annual anthropogenic CO_2 emissions, far below the equilibrium level.

The total air-sea CO_2 flux in the contemporary ocean is the sum of the air-sea flux of anthropogenic CO_2, which determines the net invasion of CO_2 into the ocean, and the large background flux of natural CO_2, which dominates the gross air-sea CO_2 exchange (**Figure 1**). The total air-sea CO_2 exchange can be estimated from measurements of air and seawater pCO_2 using bulk formulae (100, 101). Thanks to a large and growing network of seawater pCO_2 measurements from both research cruises and ships of opportunity (102, 103), we can now reconstruct the variability of the air-sea CO_2 flux at a global scale since roughly the mid-1980s using various statistical, mechanistic, or regression-based models (104–107). Comparing the average of these estimates (15) with the air-sea flux of anthropogenic CO_2, two distinct differences are clear (**Figure 6*b***). First, the total oceanic uptake of CO_2 is less than the oceanic uptake of anthropogenic CO_2. This difference indicates a net emission of natural CO_2 from the ocean. Some of this must be driven by the substantial transport of terrestrial carbon to the ocean by rivers and submarine groundwaters (10, 11), much of which is processed to DIC in the ocean and reemitted to the atmosphere. Estimates of the oceanic outgassing of terrestrially derived CO_2 range from 0.2 to 1.2 GtC year^{-1} (108, 109), but there are large uncertainties in these estimates, and it is not clear if other natural processes are causing a net influx or outflux of natural CO_2 from the ocean over the past 30 years. The second difference between the total and anthropogenic air-sea CO_2 flux is that there is more variability in the former than the latter. This variability must therefore reflect substantial variability in natural air-sea CO_2 fluxes, which has been linked both to internal climate variability (110) and to externally forced variability due to major volcanic eruptions (111).

As anthropogenic CO_2 enters the ocean and accumulates as DIC, seawater pCO_2 rises and seawater pH declines. The decline of pH due to anthropogenic DIC accumulation is known as ocean acidification (112). Over the industrial era, the average surface seawater pH has declined by nearly 0.1 pH units, with the majority of this decline occurring in the past 50 years (**Figure 6*c***). In addition to reducing the equilibrium carbon capacity of seawater, ocean acidification has the potential to adversely affect ocean ecosystems by enhancing the dissolution rates of the carbonate skeletons of some marine organisms (113). As seawater pH drops, carbonate ion (CO_3^{2-}) concentrations also drop, reducing the thermodynamic stability of $CaCO_3$ exoskeletons. This has detrimental impacts on numerous marine organisms, including corals, planktonic foraminifera and pteropods, mollusks, echinoderms, and the larval stages of fishes (114, 115). Seawater pH is predicted to reach as low as 7.8 by the end of the twenty-first century following business-as-usual emissions scenarios (116). This level of acidification could potentially result in massive die-offs of coral reefs (117) and indicates that ocean acidification is a leading threat for marine ecosystems in the twenty-first century (118).

The extent of ocean acidification is roughly proportional to the accumulation of anthropogenic DIC in the ocean, and as such the greatest declines in pH to date have occurred in the surface ocean, where the concentration of anthropogenic DIC is the highest (**Figure 7*a–c***). Because of the slow ventilation times of the deep ocean, anthropogenic DIC has not penetrated into the deep layers of many parts of the ocean. The deepest penetration of anthropogenic carbon is found in the North Atlantic (**Figure 7*b***), where upwelling in the subpolar gyre exposes deeper waters to the atmosphere where they can take up anthropogenic CO_2, and deep waters forming in the Labrador and Greenland Seas bring anthropogenic carbon into the deep ocean (119, 120). The

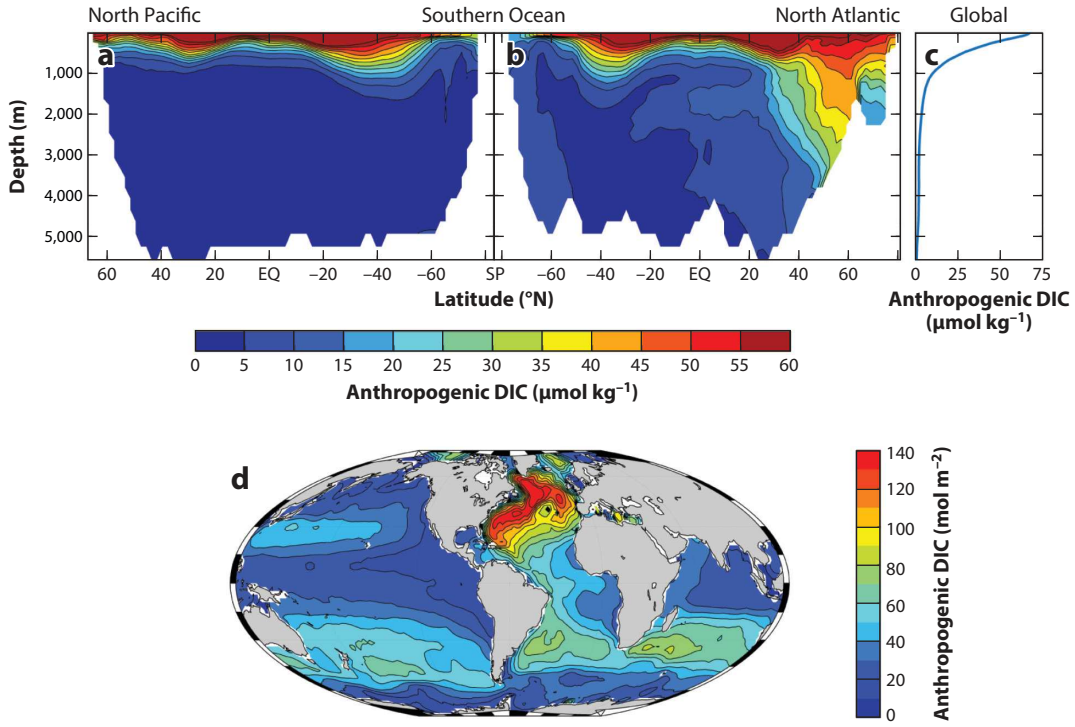

Figure 7

(*a–c*) Anthropogenic DIC concentration in the ocean as of 2018, zonally averaged in the Pacific Ocean (*a*) and the Atlantic Ocean (*b*), and a global vertical profile (*c*) showing the relatively shallow penetration of anthropogenic DIC in most parts of the ocean. (*d*) Vertically integrated column inventory of anthropogenic DIC in the ocean as of 2018. Anthropogenic DIC estimates are from an ocean circulation inverse model (41). Abbreviations: DIC, dissolved inorganic carbon; EQ, equator; SP, South Pole.

column inventory of anthropogenic DIC shows the greatest accumulation in the western North Atlantic, associated with the southward-flowing deep western boundary current (**Figure 7*d***).

Deep waters also form along the Antarctic margin, but the invasion of anthropogenic CO_2 is hindered by sea ice in this region as well as by the short residence time of upwelled waters at the surface, which reduces their capacity to equilibrate with the atmosphere (121). However, the open Southern Ocean takes up significant amounts of anthropogenic CO_2. This region is the primary conduit for deep waters upwelling to the surface (122), and as these upwelled deep waters are advected equatorward, they absorb anthropogenic CO_2 from the atmosphere (123), accounting for up to 40% of the oceanic uptake of anthropogenic CO_2 (41, 124, 125). Most of the anthropogenic CO_2 taken up in the Southern Ocean is transported into the interior ocean within northward-flowing intermediate water masses (126) and accumulates in the subpolar thermocline, leading to high anthropogenic DIC inventories at around 30°S (**Figure 7*d***).

The total accumulation of anthropogenic DIC in the ocean should not be confused with the total amount of anthropogenic CO_2 emissions that have entered the ocean. Because the ocean and atmosphere exchange CO_2 constantly, almost all anthropogenic CO_2 emissions have most probably entered the ocean at some point. However, much of this anthropogenic CO_2 is cycled through the wind-driven upper ocean circulation and evades back out to the atmosphere (127), further reinforcing the idea that subduction of anthropogenic DIC into the ocean's deeper layers is the rate-limiting step on oceanic anthropogenic CO_2 uptake.

5. THE FUTURE OF THE OCEANIC CARBON SINK

The ocean provides a critical climate service by absorbing much of the CO_2 emitted by industrial activities, but this is challenged by the magnitude of the human disturbance of the natural carbon cycle and the slow rate of ocean overturning, which limits the rate of oceanic CO_2 uptake, as well as the continued acidification of the ocean, which reduces its equilibrium capacity to absorb CO_2. The future of the ocean carbon sink is in some respects well charted, while in others significant uncertainties remain. Here I outline some of the key knowns and unknowns regarding how the ocean carbon cycle will respond to continued anthropogenic perturbations over the next century.

Stratification: a measure of the vertical gradient of density in the ocean, with larger stratification indicating greater stability of the water column and reduced capacity for convection

The primary, well-understood response of the ocean to ongoing industrial CO_2 emissions is absorption of anthropogenic CO_2, which causes ocean acidification and a reduction of the equilibrium carbon capacity of the ocean. The chemical equilibrium effects are well understood, and the ocean is predicted to absorb approximately 85% of human fossil fuel emissions, depending on the cumulative amount of CO_2 emitted. This will be modified to some extent by warming of the ocean, which reduces the solubility of CO_2 and is projected to reduce oceanic CO_2 uptake by ~10% relative to nonwarming scenarios (128). The key unknowns with regard to these well-understood chemical effects are the total amount of CO_2 that will be emitted by industrial activities prior to decarbonization and the total surface warming that will occur due to CO_2 radiative effects (129).

The second most important influence on the evolution of the ocean carbon cycle in the twenty-first century is the response of the ocean's overturning circulation to anthropogenic warming. Numerous modeling studies predict that the ocean's overturning circulation will weaken as the ocean becomes warmer and more stratified, which reduces deep convection in high latitudes (130–132). The initial response of the carbon cycle to a reduction in overturning circulation is an increase in the strength of the biological carbon pump driven by increased trapping of respired carbon in the subsurface ocean (130, 133). At the same time, however, the rate of oceanic anthropogenic CO_2 uptake is reduced as the overturning circulation weakens and less anthropogenic DIC is transported into the ocean's deeper layers (130, 131). Over time, most models predict that the reduction of anthropogenic CO_2 uptake outweighs the increase in biological carbon storage, and thus reduced overturning has the overall effect of weakening the ocean carbon sink (130, 131, 134).

A knock-on effect of enhanced ocean stratification and reduced overturning is that the supply of nutrients to surface waters from the mixing and upwelling of deep waters is reduced. Models suggest that this reduction in nutrient supply, combined with warmer ocean surface temperatures, will drive declining biological productivity in the surface ocean and declining carbon export (69, 135). Some models project drastic reductions in marine ecosystem productivity due to semicollapsed overturning circulation several hundred years in the future (136). This projected reduction in carbon export weakens the biological carbon pump, working against the effects of slower overturning circulation that serve to trap more respired carbon in the deep ocean. The total strength of the biological pump can be expressed as the product of the carbon export and the sequestration time of respired carbon in the deep ocean (83), with weaker overturning leading to longer sequestration times. It is not clear which of these opposing effects, the reduction in carbon export or the increase in the sequestration time of respired carbon, will be more important and therefore how the strength of the ocean's biological carbon pump will change in the future. Resolution of this issue requires a better understanding of the sensitivity of ocean carbon export to climate change (137, 138).

A final consideration is whether deliberate human interventions can or will have an impact on the trajectory of the ocean carbon cycle in the next century. Interest is building in geoengineering approaches to combat CO_2-induced global warming by manipulating the ocean's natural carbon cycle (139). These approaches generally fall under one of two categories: enhancing the rate at which DIC is transferred from the surface ocean or atmosphere to the deep ocean or manipulating

the chemistry of the ocean to increase its carbon-buffering capacity. Examples of the former include enhancing ocean productivity and carbon export by adding fertilizing nutrients such as iron to seawater (140) or ocean afforestation via seaweed farming (141), while examples of the latter include the deliberate dissolution of minerals in seawater to change the acid-base balance toward a more alkaline and higher-pH ocean (142). A full analysis of these strategies can be found in other reviews (143), but they all involve speeding up natural processes in the ocean carbon cycle. Approaches such as ocean fertilization or afforestation enhance the transfer of carbon from the surface ocean to the deep ocean and thereby speed up the rate at which the ocean takes up anthropogenic CO_2, which is otherwise naturally controlled by the ocean's overturning circulation over centennial to millennial timescales. Ocean alkalinization mimics natural weathering processes that would naturally work to gradually restore the ocean's carbon-buffering capacity on timescales of tens of thousands to millions of years (22). Thus, these schemes cannot change the ultimate response of the ocean or the atmosphere to anthropogenic CO_2 emissions.

SUMMARY POINTS

1. The ocean controls the atmospheric CO_2 concentration on timescales of decades to millennia, and the equilibrium partitioning of carbon between the ocean and atmosphere is determined by the relative mass of the ocean and atmosphere, the chemical carbon capacity of the ocean, and the magnitude of the ocean carbon pumps.
2. Conceptual models, ocean biogeochemical models, and modern dissolved inorganic carbon (DIC) observations all suggest that the biological pump increases the ocean DIC inventory by almost 10% (2,800 GtC), reducing atmospheric CO_2 by roughly half.
3. The ocean at present absorbs CO_2 at a rate that is equivalent to roughly 25% of anthropogenic CO_2 emissions, well below its theoretical maximum capacity of 85% due to the slow rate of ocean overturning circulation.
4. Several feedbacks will work to weaken the rate of anthropogenic CO_2 uptake in the future, including ocean acidification, which reduces the equilibrium carbon capacity of seawater; ocean warming, which reduces the CO_2 solubility; and slowing ocean overturning circulation, which reduces the rate at which anthropogenic CO_2 penetrates into the deeper ocean.
5. Uncertainty in the rate at which the ocean will absorb CO_2 in the coming decades is mainly due to uncertainties in how ocean circulation will respond to climate change, with potentially large and often opposing effects on the air-sea carbon balance through its effects on carbon export, the sequestration time of biological carbon, and the subduction of anthropogenic CO_2 into the deep ocean.

FUTURE ISSUES

1. Anthropogenic CO_2 uptake is reasonably well quantified for the contemporary ocean but is sensitive to ongoing changes in the ocean's overturning circulation. Continued observations of changes in the oceanic DIC inventory and development of high-resolution models that can accurately capture ocean circulation changes in response to climate

change will be needed to provide accurate estimates of ocean anthropogenic CO_2 uptake moving forward.

2. The gross air-sea CO_2 flux is dominated by naturally occurring CO_2, and these fluxes may be highly sensitive to ongoing climate change, including changes in ocean circulation, the biological carbon pump, and the transport of carbon from terrestrial ecosystems into the ocean. Sustained and intensive measurements of seawater pCO_2 throughout the ocean are required in order to assess the magnitude of natural ocean CO_2 emissions to the atmosphere, and how they are changing with time.
3. The response of the ocean's biological systems to climate change is very poorly understood. A better understanding of the mechanisms and magnitudes of the ocean's biological carbon pump is needed to gauge how ocean productivity, carbon export, and carbon storage by the biological pump will behave in a changing climate.
4. Geoengineering of the ocean carbon sink may be useful for mitigating climate change due to rising CO_2 levels by enhancing the rate of oceanic CO_2 uptake, but geoengineering approaches cannot change the equilibrium partitioning of carbon between the ocean and atmosphere. Abating industrial CO_2 emissions is the only permanent solution to reducing atmospheric CO_2 levels.

DISCLOSURE STATEMENT

The author is not aware of any affiliations, memberships, funding, or financial holdings that might be perceived as affecting the objectivity of this review.

ACKNOWLEDGMENTS

The author acknowledges support from the US National Science Foundation through grant OCE-1948955.

LITERATURE CITED

1. Bolin B. 1970. The carbon cycle. *Sci. Am.* 223(3):124–35
2. Kump LR, Brantley SL, Arthur MA. 2000. Chemical weathering, atmospheric CO_2, and climate. *Annu. Rev. Earth Planet. Sci.* 28:611–67
3. Crowley TJ, Berner RA. 2001. CO_2 and climate change. *Science* 292(5518):870–72
4. Berner R, Lasaga A, Garrels R. 1983. Carbonate-silicate geochemical cycle and its effect on atmospheric carbon dioxide over the past 100 million years. *Am. J. Sci.* 283(7):641–83
5. Bar-On YM, Phillips R, Milo R. 2018. The biomass distribution on earth. *PNAS* 115(25):6506–11
6. Scharlemann JP, Tanner EV, Hiederer R, Kapos V. 2014. Global soil carbon: understanding and managing the largest terrestrial carbon pool. *Carbon Manag.* 5(1):81–91
7. Burton MR, Sawyer GM, Granieri D. 2013. Deep carbon emissions from volcanoes. *Rev. Mineral. Geochem.* 75(1):323–54
8. Gaillardet J, Dupré B, Louvat P, Allegre C. 1999. Global silicate weathering and CO_2 consumption rates deduced from the chemistry of large rivers. *Chem. Geol.* 159(1–4):3–30
9. Cartapanis O, Galbraith ED, Bianchi D, Jaccard SL. 2018. Carbon burial in deep-sea sediment and implications for oceanic inventories of carbon and alkalinity over the last glacial cycle. *Climate Past* 14(11):1819–50
10. Bauer JE, Cai WJ, Raymond PA, Bianchi TS, Hopkinson CS, Regnier PA. 2013. The changing carbon cycle of the coastal ocean. *Nature* 504(7478):61–70

11. Regnier P, Resplandy L, Najjar RG, Ciais P. 2022. The land-to-ocean loops of the global carbon cycle. *Nature* 603(7901):401–10
12. Friedlingstein P, Jones MW, O'Sullivan M, Andrew RM, Hauck J, et al. 2019. Global Carbon Budget 2019. *Earth Syst. Sci. Data* 11(4):1783–838
13. Ito A. 2011. A historical meta-analysis of global terrestrial net primary productivity: Are estimates converging? *Glob. Change Biol.* 17(10):3161–75
14. Field CB, Behrenfeld MJ, Randerson JT, Falkowski P. 1998. Primary production of the biosphere: integrating terrestrial and oceanic components. *Science* 281(5374):237–40
15. Friedlingstein P, O'Sullivan M, Jones MW, Andrew RM, Hauck J, et al. 2020. Global Carbon Budget 2020. *Earth Syst. Sci. Data* 12(4):3269–340
16. Revelle R, Suess HE. 1957. Carbon dioxide exchange between atmosphere and ocean and the question of an increase of atmospheric CO_2 during the past decades. *Tellus* 9(1):18–27
17. Broecker WS. 1982. Glacial to interglacial changes in ocean chemistry. *Prog. Oceanogr.* 11(2):151–97
18. Keeling CD, Bacastow RB, Bainbridge AE, Ekdahl CA Jr., Guenther PR, et al. 1976. Atmospheric carbon dioxide variations at Mauna Loa observatory, Hawaii. *Tellus* 28(6):538–51
19. Nevison CD, Mahowald NM, Doney SC, Lima ID, Van der Werf GR, et al. 2008. Contribution of ocean, fossil fuel, land biosphere, and biomass burning carbon fluxes to seasonal and interannual variability in atmospheric CO_2. *J. Geophys. Res. Biogeosci.* 113(G1):G01010
20. MacFarling Meure C, Etheridge D, Trudinger C, Steele P, Langenfelds R, et al. 2006. Law Dome CO_2, CH_4 and N_2O ice core records extended to 2000 years BP. *Geophys. Res. Lett.* 33:L14810
21. Keeling CD, Piper SC, Bacastow RB, Wahlen M, Whorf TP, et al. 2001. Exchanges of atmospheric CO_2 and $^{13}CO_2$ with the terrestrial biosphere and oceans from 1978 to 2000. I. Global aspects. *SIO Ref. Ser.* 1–6. **https://escholarship.org/uc/item/09v319r9**
22. Archer D. 2005. Fate of fossil fuel CO_2 in geologic time. *J. Geophys. Res. Oceans* 110(C9):C09S05
23. Dickens GR. 2003. Rethinking the global carbon cycle with a large, dynamic and microbially mediated gas hydrate capacitor. *Earth Planet. Sci. Lett.* 213(3–4):169–83
24. Hansell DA. 2013. Recalcitrant dissolved organic carbon fractions. *Annu. Rev. Mar. Sci.* 5:421–45
25. Buch K. 1933. Der borsäuregehalt des meerwassers und seine bedeutung bei der berechnung des kohlensäuresystems im meerwasser [The boric acid content of seawater and its importance in the calculation of the carbonic acid system in seawater]. *Rapp. Cons. Explor. Mer.* 85:71–75
26. Lyman J. 1972. 38.—Development of ideas concerning the carbon dioxide system in sea water up to 1940. *Proc. R. Soc. Edinburgh Sect. B Biol. Sci.* 72(1):381–87
27. Mehrbach C, Culberson C, Hawley J, Pytkowicx R. 1973. Measurement of the apparent dissociation constants of carbonic acid in seawater at atmospheric pressure 1. *Limnol. Oceanogr.* 18(6):897–907
28. Dickson A, Millero FJ. 1987. A comparison of the equilibrium constants for the dissociation of carbonic acid in seawater media. *Deep Sea Res. Part A Oceanogr. Res. Pap.* 34(10):1733–43
29. Broecker WS, Peng TH. 1974. Gas exchange rates between air and sea. *Tellus* 26(1–2):21–35
30. Wanninkhof R. 1992. Relationship between wind speed and gas exchange over the ocean. *J. Geophys. Res. Oceans* 97(C5):7373–82
31. Weiss R. 1974. Carbon dioxide in water and seawater: the solubility of a non-ideal gas. *Mar. Chem.* 2(3):203–15
32. Zeebe RE, Wolf-Gladrow D. 2001. *CO_2 in Seawater: Equilibrium, Kinetics, and Isotopes*. Elsevier Oceanogr. Ser. 65. Amsterdam: Elsevier Sci.
33. Egleston ES, Sabine CL, Morel FM. 2010. Revelle revisited: buffer factors that quantify the response of ocean chemistry to changes in DIC and alkalinity. *Glob. Biogeochem. Cycles* 24(1):GB1002
34. Broecker WS, Takahashi T, Simpson H, Peng TH. 1979. Fate of fossil fuel carbon dioxide and the global carbon budget. *Science* 206(4417):409–18
35. Lefevre N, Ciabrini J, Michard G, Brient B, DuChaffaut M, Merlivat L. 1993. A new optical sensor for pCO_2 measurements in seawater. *Mar. Chem.* 42(3–4):189–98
36. Lauvset SK, Lange N, Tanhua T, Bittig HC, Olsen A, et al. 2021. An updated version of the global interior ocean biogeochemical data product, GLODAPv2.2021. *Earth Syst. Sci. Data* 13(12):5565–89
37. Lewis E, Wallace D. 1998. *Program developed for CO_2 system calculations*. Tech. Rep., Environ. Syst. Sci. Data Infrastruct. Virtual Ecosyst., US Off. Sci. Tech. Inf., Washington, DC

38. Emerson S, Hedges J. 2008. *Chemical Oceanography and the Marine Carbon Cycle*. Cambridge, UK: Cambridge Univ. Press
39. Eakins BW, Sharman GF. 2010. *Volumes of the world's oceans from ETOPO1*. NOAA Natl. Geophys. Data Ctr., Boulder, CO
40. Trenberth KE, Smith L. 2005. The mass of the atmosphere: a constraint on global analyses. *J. Climate* 18(6):864–75
41. DeVries T. 2014. The oceanic anthropogenic CO_2 sink: storage, air-sea fluxes, and transports over the industrial era. *Glob. Biogeochem. Cycles* 28(7):631–47
42. Volk T, Hoffert MI. 1985. Ocean carbon pumps: analysis of relative strengths and efficiencies in ocean-driven atmospheric CO_2 changes. In *The Carbon Cycle and Atmospheric CO_2: Natural Variations Archean to Present*, ed. ET Sundquist, WS Broecker, pp. 99–110. Geophys. Monogr. Ser. 32, Washington, DC: Am. Geophys. Union
43. Broecker WS. 1982. Ocean chemistry during glacial time. *Geochim. Cosmochim. Acta* 46(10):1689–705
44. Martin JH. 1990. Glacial-interglacial CO_2 change: the iron hypothesis. *Paleoceanography* 5(1):1–13
45. Sigman DM, Boyle EA. 2000. Glacial/interglacial variations in atmospheric carbon dioxide. *Nature* 407(6806):859–69
46. Bolin B, Eriksson E. 1959. Changes in the carbon dioxide content of the atmosphere and sea due to fossil fuel combustion. *Atmos. Sea Motion* 1:30–142
47. Emery W, Meincke J. 1986. Global water masses: summary and review. *Oceanolog. Acta* 9(4):383–91
48. Gordon A. 2001. Bottom water formation. In *Encyclopedia of Ocean Sciences*, ed. JH Steele, SA Thorpe, KK Turekian, pp. 415–21. San Diego, CA: Academic Press. 2nd ed.
49. Ito T, Follows MJ. 2003. Upper ocean control on the solubility pump of CO_2. *J. Mar. Res.* 61(4):465–89
50. Toggweiler J, Gnanadesikan A, Carson S, Murnane R, Sarmiento JL. 2003. Representation of the carbon cycle in box models and GCMs: 1. Solubility pump. *Glob. Biogeochem. Cycles* 17:1026
51. DeVries T, Primeau F. 2009. Atmospheric pCO_2 sensitivity to the solubility pump: role of the low-latitude ocean. *Glob. Biogeochem. Cycles* 23(4):GB4020
52. Murnane R, Sarmiento JL, Le Quéré C. 1999. Spatial distribution of air-sea CO_2 fluxes and the interhemispheric transport of carbon by the oceans. *Glob. Biogeochem. Cycles* 13(2):287–305
53. Sarmiento JL, Gruber N. 2013. *Ocean Biogeochemical Dynamics*. Princeton, NJ: Princeton Univ. Press
54. Wanninkhof R, Park GH, Takahashi T, Sweeney C, Feely R, et al. 2013. Global ocean carbon uptake: magnitude, variability and trends. *Biogeosciences* 10(3):1983–2000
55. Wu Y, Hain MP, Humphreys MP, Hartman S, Tyrrell T. 2019. What drives the latitudinal gradient in open-ocean surface dissolved inorganic carbon concentration? *Biogeosciences* 16(13):2661–81
56. Broecker WS. 1991. The great ocean conveyor. *Oceanography* 4:79–89
57. Lozier MS. 2010. Deconstructing the conveyor belt. *Science* 328(5985):1507–11
58. DeVries T, Holzer M. 2019. Radiocarbon and helium isotope constraints on deep ocean ventilation and mantle-^{3}He sources. *J. Geophys. Res. Oceans* 124(5):3036–57
59. Khatiwala S, Primeau F, Holzer M. 2012. Ventilation of the deep ocean constrained with tracer observations and implications for radiocarbon estimates of ideal mean age. *Earth Planet. Sci. Lett.* 325:116–25
60. Galbraith ED, Skinner LC. 2020. The biological pump during the last glacial maximum. *Annu. Rev. Mar. Sci.* 12:559–86
61. Kwon EY, Sarmiento JL, Toggweiler J, DeVries T. 2011. The control of atmospheric pCO_2 by ocean ventilation change: the effect of the oceanic storage of biogenic carbon. *Glob. Biogeochem. Cycles* 25(3):GB3026
62. Marinov I, Gnanadesikan A, Sarmiento JL, Toggweiler J, Follows M, Mignone B. 2008. Impact of oceanic circulation on biological carbon storage in the ocean and atmospheric pCO_2. *Glob. Biogeochem. Cycles* 22(3):GB3007
63. Ito T, Follows MJ. 2005. Preformed phosphate, soft tissue pump and atmospheric CO_2. *J. Mar. Res.* 63(4):813–39
64. Elderfield H. 2002. Carbonate mysteries. *Science* 296(5573):1618–21
65. Lee Z, Weidemann A, Kindle J, Arnone R, Carder KL, Davis C. 2007. Euphotic zone depth: its derivation and implication to ocean-color remote sensing. *J. Geophys. Res. Oceans* 112(C3):C03009

66. Falkowski PG, Barber RT, Smetacek V. 1998. Biogeochemical controls and feedbacks on ocean primary production. *Science* 281(5374):200–6
67. Schlitzer R. 2002. Carbon export fluxes in the Southern Ocean: results from inverse modeling and comparison with satellite-based estimates. *Deep Sea Res. Part II Top. Stud. Oceanogr.* 49(9–10):1623–44
68. DeVries T, Weber T. 2017. The export and fate of organic matter in the ocean: new constraints from combining satellite and oceanographic tracer observations. *Glob. Biogeochem. Cycles* 31(3):535–55
69. Laws EA, Falkowski PG, Smith WO Jr., Ducklow H, McCarthy JJ. 2000. Temperature effects on export production in the open ocean. *Glob. Biogeochem. Cycles* 14(4):1231–46
70. Dunne JP, Sarmiento JL, Gnanadesikan A. 2007. A synthesis of global particle export from the surface ocean and cycling through the ocean interior and on the seafloor. *Glob. Biogeochem. Cycles* 21(4):GB4006
71. Siegel DA, Buesseler KO, Behrenfeld MJ, Benitez-Nelson CR, Boss E, et al. 2016. Prediction of the export and fate of global ocean net primary production: the EXPORTS science plan. *Front. Mar. Sci.* 3:22
72. Alldredge AL, Gotschalk C. 1989. Direct observations of the mass flocculation of diatom blooms: characteristics, settling velocities and formation of diatom aggregates. *Deep Sea Res. Part A Oceanogr. Res. Pap.* 36(2):159–71
73. Steinberg DK, Landry MR. 2017. Zooplankton and the ocean carbon cycle. *Annu. Rev. Mar. Sci.* 9:413–44
74. Saba GK, Burd AB, Dunne JP, Hernández-León S, Martin AH, et al. 2021. Toward a better understanding of fish-based contribution to ocean carbon flux. *Limnol. Oceanogr.* 66(5):1639–64
75. Bianchi D, Carozza DA, Galbraith ED, Guiet J, DeVries T. 2021. Estimating global biomass and biogeochemical cycling of marine fish with and without fishing. *Sci. Adv.* 7(41):eabd7554
76. Roshan S, DeVries T. 2017. Efficient dissolved organic carbon production and export in the oligotrophic ocean. *Nat. Commun.* 8:2036
77. Dall'Olmo G, Dingle J, Polimene L, Brewin RJ, Claustre H. 2016. Substantial energy input to the mesopelagic ecosystem from the seasonal mixed-layer pump. *Nat. Geosci.* 9(11):820–23
78. Omand MM, D'Asaro EA, Lee CM, Perry MJ, Briggs N, et al. 2015. Eddy-driven subduction exports particulate organic carbon from the spring bloom. *Science* 348(6231):222–25
79. Steinberg DK, Carlson CA, Bates NR, Goldthwait SA, Madin LP, Michaels AF. 2000. Zooplankton vertical migration and the active transport of dissolved organic and inorganic carbon in the Sargasso Sea. *Deep Sea Res. Part I Oceanogr. Res. Pap.* 47(1):137–58
80. Davison P, Checkley D Jr., Koslow J, Barlow J. 2013. Carbon export mediated by mesopelagic fishes in the northeast Pacific Ocean. *Prog. Oceanogr.* 116:14–30
81. Schiebel R. 2002. Planktic foraminiferal sedimentation and the marine calcite budget. *Glob. Biogeochem. Cycles* 16(4):1065
82. Buitenhuis ET, Le Quéré C, Bednaršek N, Schiebel R. 2019. Large contribution of pteropods to shallow $CaCO_3$ export. *Glob. Biogeochem. Cycles* 33(3):458–68
83. DeVries T, Primeau F, Deutsch C. 2012. The sequestration efficiency of the biological pump. *Geophys. Res. Lett.* 39(13):L13601
84. Boyd PW, Claustre H, Levy M, Siegel DA, Weber T. 2019. Multi-faceted particle pumps drive carbon sequestration in the ocean. *Nature* 568(7752):327–35
85. Redfield AC. 1958. The biological control of chemical factors in the environment. *Am. Sci.* 46(3):205–21
86. Carter B, Feely R, Lauvset S, Olsen A, DeVries T, Sonnerup R. 2021. Preformed properties for marine organic matter and carbonate mineral cycling quantification. *Glob. Biogeochem. Cycles* 35(1):e2020GB006623
87. Nowicki M, DeVries T, Siegel DA. 2022. Quantifying the carbon export and sequestration pathways of the ocean's biological carbon pump. *Glob. Biogeochem. Cycles* 36(3):e2021GB007083
88. Ito T, Follows MJ. 2013. Air-sea disequilibrium of carbon dioxide enhances the biological carbon sequestration in the Southern Ocean. *Glob. Biogeochem. Cycles* 27(4):1129–38
89. Eggleston S, Galbraith ED. 2018. The devil's in the disequilibrium: multi-component analysis of dissolved carbon and oxygen changes under a broad range of forcings in a general circulation model. *Biogeosciences* 15(12):3761–77

90. Gruber N, Sarmiento JL. 2002. Large-scale biogeochemical-physical interactions in elemental cycles. In *The Sea*, Vol. 12, ed. A Robinson, JJ McCarthy, BJ Rothschild, pp. 337–99. Cambridge, MA: Harvard Univ. Press
91. Chen CTA. 1982. On the distribution of anthropogenic CO_2 in the Atlantic and Southern Oceans. *Deep Sea Res. Part A Oceanogr. Res. Pap.* 29(5):563–80
92. Gruber N, Sarmiento JL, Stocker TF. 1996. An improved method for detecting anthropogenic CO_2 in the oceans. *Glob. Biogeochem. Cycles* 10(4):809–37
93. Sabine CL, Feely RA, Gruber N, Key RM, Lee K, et al. 2004. The oceanic sink for anthropogenic CO_2. *Science* 305(5682):367–71
94. Khatiwala S, Tanhua T, Mikaloff Fletcher S, Gerber M, Doney SC, et al. 2013. Global ocean storage of anthropogenic carbon. *Biogeosciences* 10(4):2169–91
95. Gruber N, Clement D, Carter BR, Feely RA, Van Heuven S, et al. 2019a. The oceanic sink for anthropogenic CO_2 from 1994 to 2007. *Science* 363(6432):1193–99
96. Holzer M, DeVries T, de Lavergne C. 2021. Diffusion controls the ventilation of a Pacific Shadow Zone above abyssal overturning. *Nat. Commun.* 12(1):4348
97. Univ. Hawai'i. 2021. Hawaii ocean time-series data organization & graphical system (HOT-DOGS). *University of Hawai'i at Manoa*. **https://hahana.soest.hawaii.edu/hot/hot-dogs/interface.html**, accessed on October 28, 2021
98. Williams RG, Roussenov V, Goodwin P, Resplandy L, Bopp L. 2017. Sensitivity of global warming to carbon emissions: effects of heat and carbon uptake in a suite of Earth system models. *J. Climate* 30(23):9343–63
99. Sarmiento JL, Orr JC, Siegenthaler U. 1992. A perturbation simulation of CO_2 uptake in an ocean general circulation model. *J. Geophys. Res. Oceans* 97(C3):3621–45
100. Takahashi T, Feely RA, Weiss RF, Wanninkhof RH, Chipman DW, et al. 1997. Global air-sea flux of CO_2: an estimate based on measurements of sea–air pCO_2 difference. *PNAS* 94(16):8292–99
101. Takahashi T, Sutherland SC, Sweeney C, Poisson A, Metzl N, et al. 2002. Global sea–air CO_2 flux based on climatological surface ocean pCO_2, and seasonal biological and temperature effects. *Deep Sea Res. Part II Top. Stud. Oceanogr.* 49(9–10):1601–22
102. Pfeil B, Olsen A, Bakker DC, Hankin S, Koyuk H, et al. 2013. A uniform, quality controlled Surface Ocean CO_2 Atlas (SOCAT). *Earth Syst. Sci. Data* 5(1):125–43
103. Bakker DC, Pfeil B, Landa CS, Metzl N, O'brien KM, et al. 2016. A multi-decade record of high-quality fCO_2 data in version 3 of the Surface Ocean CO_2 Atlas (SOCAT). *Earth Syst. Sci. Data* 8(2):383–413
104. Denvil-Sommer A, Gehlen M, Vrac M, Mejia C. 2019. LSCE-FFNN-v1: a two-step neural network model for the reconstruction of surface ocean pCO_2 over the global ocean. *Geosci. Model Dev.* 12(5):2091–105
105. Gregor L, Lebehot AD, Kok S, Scheel Monteiro PM. 2019. A comparative assessment of the uncertainties of global surface ocean CO_2 estimates using a machine-learning ensemble (CSIR-ML6 version 2019a)—Have we hit the wall? *Geosci. Model Dev.* 12(12):5113–36
106. Landschuetzer P, Gruber N, Bakker DC. 2016. Decadal variations and trends of the global ocean carbon sink. *Glob. Biogeochem. Cycles* 30(10):1396–417
107. Rödenbeck C, Bakker DC, Metzl N, Olsen A, Sabine C, et al. 2014. Interannual sea–air CO_2 flux variability from an observation-driven ocean mixed-layer scheme. *Biogeosciences* 11(17):4599–613
108. Lacroix F, Ilyina T, Hartmann J. 2020. Oceanic CO_2 outgassing and biological production hotspots induced by pre-industrial river loads of nutrients and carbon in a global modeling approach. *Biogeosciences* 17(1):55–88
109. Kwon EY, DeVries T, Galbraith ED, Hwang J, Kim G, Timmermann A. 2021. Stable carbon isotopes suggest large terrestrial carbon inputs to the global ocean. *Glob. Biogeochem. Cycles* 35(4):e2020GB006684
110. Landschützer P, Gruber N, Haumann FA, Rödenbeck C, Bakker DC, et al. 2015. The reinvigoration of the Southern Ocean carbon sink. *Science* 349(6253):1221–24
111. McKinley GA, Fay AR, Eddebbar YA, Gloege L, Lovenduski NS. 2020. External forcing explains recent decadal variability of the ocean carbon sink. *AGU Adv.* 1(2):e2019AV000149
112. Doney SC, Fabry VJ, Feely RA, Kleypas JA. 2009. Ocean acidification: the other CO_2 problem. *Annu. Rev. Mar. Sci.* 1:169–92

113. Roleda MY, Boyd PW, Hurd CL. 2012. Before ocean acidification: calcifier chemistry lessons 1. *J. Phycol.* 48(4):840–43
114. Fabry VJ, Seibel BA, Feely RA, Orr JC. 2008. Impacts of ocean acidification on marine fauna and ecosystem processes. *ICES J. Mar. Sci.* 65(3):414–32
115. Wittmann AC, Pörtner HO. 2013. Sensitivities of extant animal taxa to ocean acidification. *Nat. Climate Change* 3(11):995–1001
116. Feely RA, Doney SC, Cooley SR. 2009. Ocean acidification: present conditions and future changes in a high-CO_2 world. *Oceanography* 22(4):36–47
117. Hoegh-Guldberg O, Mumby PJ, Hooten AJ, Steneck RS, Greenfield P, et al. 2007. Coral reefs under rapid climate change and ocean acidification. *Science* 318(5857):1737–42
118. Gruber N. 2011. Warming up, turning sour, losing breath: ocean biogeochemistry under global change. *Philos. Trans. R. Soc. A Math. Phys. Eng. Sci.* 369(1943):1980–96
119. Rhein M, Steinfeldt R, Kieke D, Stendardo I, Yashayaev I. 2017. Ventilation variability of Labrador Sea Water and its impact on oxygen and anthropogenic carbon: a review. *Philos. Trans. R. Soc. A Math. Phys. Eng. Sci.* 375(2102):20160321
120. Vazquez-Rodriguez M, Touratier F, Monaco CL, Waugh D, Padin XA, et al. 2009. Anthropogenic carbon distributions in the Atlantic Ocean: data-based estimates from the Arctic to the Antarctic. *Biogeosciences* 6(3):439–51
121. Poisson A, Chen CTA. 1987. Why is there little anthropogenic CO_2 in the Antarttic bottom water? *Deep Sea Res. Part A Oceanogr. Res. Papers* 34(7):1255–75
122. DeVries T, Primeau F. 2011. Dynamically and observationally constrained estimates of water-mass distributions and ages in the global ocean. *J. Phys. Oceanogr.* 41(12):2381–401
123. Gruber N, Landschützer P, Lovenduski NS. 2019b. The variable Southern Ocean carbon sink. *Annu. Rev. Mar. Sci.* 11:159–86
124. Khatiwala S, Primeau F, Hall T. 2009. Reconstruction of the history of anthropogenic CO_2 concentrations in the ocean. *Nature* 462(7271):346–49
125. Mikaloff Fletcher SE, Gruber N, Jacobson AR, Doney SC, Dutkiewicz S, et al. 2006. Inverse estimates of anthropogenic CO_2 uptake, transport, and storage by the ocean. *Glob. Biogeochem. Cycles* 20(2):GB2002
126. Ito T, Woloszyn M, Mazloff M. 2010. Anthropogenic carbon dioxide transport in the Southern Ocean driven by Ekman flow. *Nature* 463(7277):80–83
127. Iudicone D, Rodgers KB, Plancherel Y, Aumont O, Ito T, et al. 2016. The formation of the ocean's anthropogenic carbon reservoir. *Sci. Rep.* 6:35473
128. Plattner GK, Joos F, Stocker T, Marchal O. 2001. Feedback mechanisms and sensitivities of ocean carbon uptake under global warming. *Tellus B Chem. Phys. Meteorol.* 53(5):564–92
129. Lee J, Marotzke J, Bala G, Cao L, Corti S, et al. 2021. Future global climate: scenario-based projections and near-term information. In *Climate Change 2021: the Physical Science Basis: Contribution of Working Group I to the Sixth Assessment Report of the Intergovernmental Panel on Climate Change*, ed. V Masson-Delmotte, P Zhai, A Pirani, SL Connors, C Pean, et al., pp. 1–195. Geneva, Switz.: Int. Panel Climate Change
130. Bernardello R, Marinov I, Palter JB, Galbraith ED, Sarmiento JL. 2014. Impact of Weddell sea deep convection on natural and anthropogenic carbon in a climate model. *Geophys. Res. Lett.* 41(20):7262–69
131. Matear RJ, Hirst AC. 1999. Climate change feedback on the future oceanic CO_2 uptake. *Tellus B* 51(3):722–33
132. Holzer M, Chamberlain MA, Matear RJ. 2020. Climate-driven changes in the ocean's ventilation pathways and time scales diagnosed from transport matrices. *J. Geophys. Res. Oceans* 125(10):e2020JC016414
133. Ito T, Bracco A, Deutsch C, Frenzel H, Long M, Takano Y. 2015. Sustained growth of the Southern Ocean carbon storage in a warming climate. *Geophys. Res. Lett.* 42(11):4516–22
134. Sarmiento JL, Le Quéré C. 1996. Oceanic carbon dioxide uptake in a model of century-scale global warming. *Science* 274(5291):1346–50
135. Bopp L, Resplandy L, Orr JC, Doney SC, Dunne JP, et al. 2013. Multiple stressors of ocean ecosystems in the 21st century: projections with CMIP5 models. *Biogeosciences* 10(10):6225–45
136. Moore JK, Fu W, Primeau F, Britten GL, Lindsay K, et al. 2018. Sustained climate warming drives declining marine biological productivity. *Science* 359(6380):1139–43

137. Riebesell U, Körtzinger A, Oschlies A. 2009. Sensitivities of marine carbon fluxes to ocean change. *PNAS* 106(49):20602–9
138. Henson SA, Laufkötter C, Leung S, Giering SL, Palevsky HI, Cavan EL. 2022. Uncertain response of ocean biological carbon export in a changing world. *Nat. Geosci.* 15:248–54
139. Gattuso JP, Williamson P, Duarte CM, Magnan AK. 2021. The potential for ocean-based climate action: negative emissions technologies and beyond. *Front. Climate* 2:37
140. Buesseler KO, Doney SC, Karl DM, Boyd PW, Caldeira K, et al. 2008. Ocean iron fertilization—moving forward in a sea of uncertainty. *Science* 319(5860):162
141. Bach LT, Tamsitt V, Gower J, Hurd CL, Raven JA, Boyd PW. 2021. Testing the climate intervention potential of ocean afforestation using the Great Atlantic *Sargassum* Belt. *Nat. Commun.* 12:2556
142. Ilyina T, Wolf-Gladrow D, Munhoven G, Heinze C. 2013. Assessing the potential of calcium-based artificial ocean alkalinization to mitigate rising atmospheric CO_2 and ocean acidification. *Geophys. Res. Lett.* 40(22):5909–14
143. Keller DP, Feng EY, Oschlies A. 2014. Potential climate engineering effectiveness and side effects during a high carbon dioxide-emission scenario. *Nat. Commun.* 5:3304

Annual Review of Environment and Resources

Volume 47, 2022

Contents

II. Earth's Life Support Systems

III. Human Use of the Environment and Resources

Indexes

Errata

An online log of corrections to *Annual Review of Environment and Resources* articles may be found at http://www.annualreviews.org/errata/environ